

Steering the electron in dissociating H_2^+ via manipulating two-state population dynamics by a weak low-frequency field

Zhuo Wang,¹ Kunlong Liu,^{1,*} Pengfei Lan,^{1,2,†} and Peixiang Lu^{1,2}

¹*School of Physics and Wuhan National Laboratory for Optoelectronics, Huazhong University of Science and Technology, Wuhan 430074, China*

²*School of Science, Wuhan Institute of Technology, Wuhan 430073, China*

(Received 22 January 2015; published 27 April 2015)

We propose a scheme to steer the electron localization in dissociating H_2^+ by using the combination of a phase-stabilized few-cycle mid-infrared laser pulse and a low-frequency field. Via manipulating the population dynamics in the $1s\sigma_g$ and $2p\sigma_u$ states by the weak low-frequency field, the dissociative wave packets on these two degenerate states of opposite parities are managed to share the same kinetic energy and overlap in space. By adjusting the carrier-envelope phase of the mid-infrared pulse or simply changing the intensity of the low-frequency field, the electron localization induced by the spatial interference of the two dissociation pathways can be efficiently controlled.

DOI: [10.1103/PhysRevA.91.043419](https://doi.org/10.1103/PhysRevA.91.043419)

PACS number(s): 33.80.Rv, 42.50.Hz, 33.80.Wz

I. INTRODUCTION

The dynamics of electrons in molecules govern chemical bonds. Steering the electron in molecular dissociation in order to coherently control the dynamics of chemical reactions therefore continues to attract the attention of the atomic and molecular physics community [1–5]. With the advancement of carrier-envelope phase (CEP) stabilized few-cycle femtosecond lasers [6], the possibility of direct light-field control of a chemical reaction via steering of electronic motion has been demonstrated both theoretically [3] and experimentally [4], leading to considerable interest in the study of electron localization in molecular dissociation [7–14].

Thus far, the molecular dynamics responsible for the electron localization in dissociating H_2^+ was broadly understood as the following three steps [3,14]: (i) an ultrashort laser pulse induces the creation of a coherent nuclear wave packet on the electronic ground ($1s\sigma_g$) state or excited state ($2p\sigma_u$) of H_2^+ ; (ii) the nuclear wave packet propagates along the potential curves and towards larger internuclear distances and then is transferred between the two degenerate states by the external field; (iii) the coherent superposition of the nuclear wave packets on the two degenerate states of even and odd parities leads to the electron localization on either of the nuclei. This indicates that one can control and enhance the electron localization by synchronously or individually manipulating these three steps. Ever since the first experimental demonstration of steering electrons in molecular dissociation by a few-cycle infrared pulse [4], many schemes have been proposed to study and enhance the manipulation of electron localization [15–23]. It is shown, in both theoretical simulation [15,16] and experiments [17], that a few-cycle mid-infrared pulse is an efficient tool to control the electron localization. It is also shown that the synthesized fields can break the symmetry of the interaction and balance the

electronic and nuclear motions, ultimately leading to the enhancement of electron localization [18–20]. Besides, high asymmetry of electron localization was shown to be achieved by using the combination of a subfemtosecond pulse and a controlled field [21–23].

Basically, the asymmetric electron localization on the dissociating nuclei requires the spatial interference of dissociation pathways that lead to the degenerate states of even and odd parities and end at the same final energy [13]. Due to the dipole selection rules, however, the pathways on the states of opposite parities always involve unequal net absorption numbers of photons. For example, in the dissociation of H_2^+ the $2n$ -photon ($n \geq 0$) absorption leads to the $1s\sigma_g$ state but only the $(2n + 1)$ -photon absorption contributes to the $2p\sigma_u$ state, resulting in staggered peaks of the nuclear kinetic energy distributions of two pathways [15,24]. Therefore, in order to enhance the electron localization, the overlap in the energy distributions of dissociation pathways of opposite parities should be increased by the external field [25].

Recently, it is demonstrated that if the dissociation process is dressed by quasistatic fields, the nuclear wave packets will propagate on the Stark-shift potential energy surfaces of the $1s\sigma_g$ and $2p\sigma_u$ states [26]. Assuming that the molecule is dissociated by an infrared field and, at the same time, a low-frequency field is added during the interaction, the dynamics of the population on the lowest two states will be modulated significantly [step (iii)]. By manipulating the two-state population dynamics with the low-frequency field, we will be able to modify the kinetic energy of the population on two states and make them end at the same final energy, ultimately enhancing the electron localization. Therefore, in this paper we propose a scheme to efficiently steer the electron localization in the dissociation of H_2^+ via manipulating two-state population dynamics by using a weak low-frequency field. The combination of a phase-stabilized few-cycle midinfrared laser pulse and a weak low-frequency field is adopted. The mid-infrared pulse triggers the dissociation of H_2^+ . Then, the low-frequency field is used to manipulate the population dynamics of the $1s\sigma_g$ and $2p\sigma_u$ states. Our results show that the distributions of the nuclear kinetic energy release (KER) spectra of the

*Present address: Max Planck Institute of Microstructure Physics, Weinberg 2, 06114 Halle, Germany; liukunlong@hust.edu.cn

†pengfeilan@hust.edu.cn

two lowest-lying states are surprisingly close to each other, indicating that most of the dissociative wave packets along two pathways end at the same final kinetic energy. By adjusting the CEP, the electron localization is significantly enhanced compared to that in a single mid-infrared field. Furthermore, we show that the electron localization can also be controlled by simply changing the intensity of the low-frequency field.

II. THEORETICAL MODEL

For our numerical simulations we have used the reduced-dimensionality model (one nuclear plus one electronic degrees of freedom) of H_2^+ interacting with an intense linearly polarized pulse [27]. We assumed that the electronic and nuclear motion are restricted along the polarization direction of the pulse which is parallel to the molecular axis. Then, the time-dependent Schrödinger equation (TDSE) can be given as (Hartree atomic units, $e = m = \hbar = 1$ are used throughout unless otherwise indicated)

$$i \frac{\partial}{\partial t} \Psi(R, z; t) = H(z, R; t) \Psi(R, z; t), \quad (1)$$

where

$$H(z, R; t) = -\frac{1}{2\mu_R} \frac{\partial^2}{\partial R^2} - \frac{1}{2\mu_e} \frac{\partial^2}{\partial z^2} - \frac{1}{\sqrt{(z - R/2)^2 + \alpha}} - \frac{1}{\sqrt{(z + R/2)^2 + \alpha}} + \frac{1}{\sqrt{R^2 + \beta}} + \left(1 + \frac{1}{2m_p + 1}\right) z E(t), \quad (2)$$

where R is the internuclear distance, z is the electronic coordinate with respect to the center of mass of the two nuclei, $\mu_e = 2m_p/(2m_p + 1)$ and $\mu_R = m_p/2$ are the reduced masses with m_p as the mass of the proton, and $\alpha = 1.0$ a.u. and $\beta = 0.03$ a.u. are the soft-core parameters [28]. The pulse is defined as $E(t) = E_1 \sin(\pi t/\tau_1)^2 \sin(\omega_1 t + \phi) + E_2 \sin(\pi t/\tau_2)^2 \sin(\omega_2 t)$ being the electric field of the pulse. Here, the subscript (1,2) means the two laser-pulse components. E , τ , and ω are the peak electric field amplitude, pulse duration, and angular frequency, respectively. ϕ denotes the CEP of the 1.6- μm pulse.

The TDSE is solved on a grid by using the Crank-Nicholson method [29] with a time step of $\delta t = 0.04$ a.u. The grid is defined as $|z| \leq 300$ and $R \leq 60$ with grid spacings $\delta z = 0.2$ and $\delta R = 0.05$. The ground state of H_2^+ (electronic $1s\sigma_g$ state and $\nu = 0$ state) is chosen to be the initial state of the system and is obtained using imaginary time propagation. To suppress the nonphysical reflection from the simulation borders, we introduce the mask function in the boundary of the grid. This mask function is mainly used to absorb the ionized wave packets because the grid is big enough that the dissociative wave packets have not yet reached the boundary by the end of the interaction.

III. RESULTS AND DISCUSSION

Our control scheme has been illustrated in Fig. 1. In this scheme, we aim to drive the molecular ion to dissociation with the mid-infrared pulse and modulate two-state population

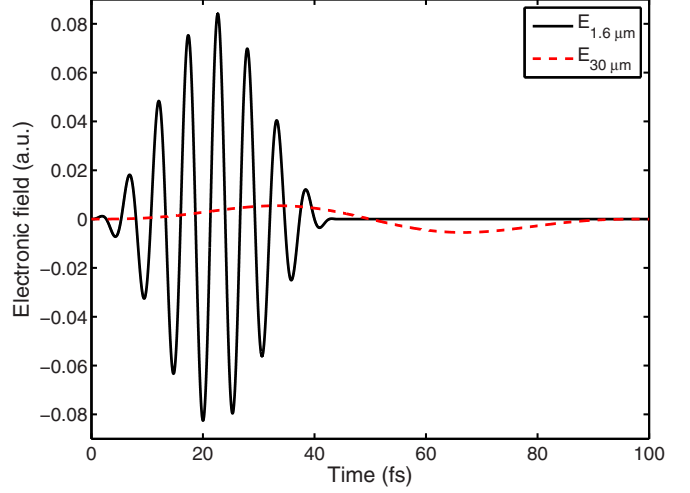


FIG. 1. (Color online) The electric field of the control scheme. The black solid (red dashed) curve shows the 1.6- μm (30- μm) field. The intensities of the two pulses are 2.5×10^{14} and 2.5×10^{12} W/cm^2 , respectively. Here, the CEP is chosen as 0π . In our scheme, the parameter ϕ is variable.

dynamics with a weak low-frequency pulse. The wavelength and intensity of the mid-infrared pulse are 1.6 μm and 2.5×10^{14} W/cm^2 , respectively. For the low-frequency field, to avoid significant ionization, we have chosen a 30- μm pulse with a weak intensity of 2.5×10^{12} W/cm^2 . The pulse durations τ_1 and τ_2 of two pulses are 44 and 100 fs, respectively. The CEP of the mid-infrared field is variable in our scheme.

First, by applying the energy window operator [30] we calculate the KER distributions of the wave packets on the two lowest-lying states as a function of CEP in the single mid-infrared (1.6- μm only) and the synthesized (1.6- and 30- μm) fields, respectively. Figures 2(a) and 2(b) show the KER distributions of the $1s\sigma_g$ and $2p\sigma_u$ states in the single mid-infrared field, respectively. In Fig. 2(c), we show a cut of the spectra at the CEP of $\phi = 0\pi$. Figures 2(d)–2(f) are the same as Figs. 2(a)–2(c), respectively, but for the synthesized field. In the single mid-infrared field, the KER distributions of the wave packets on two states are obviously different. One can see that the peaks of the KER spectra for two dissociation pathways are always staggered as the CEP changes. After adding the low-frequency field to modulate the two-state population dynamics, however, the distributions are changed significantly. From Figs. 2(d) and 2(e), we can see a bright butterfly structure in the KER distributions, which are almost symmetric. The cut of the spectra in Fig. 2(f) further shows that the KER distributions of the wave packets on the $1s\sigma_g$ and $2p\sigma_u$ states are very close to each other. This indicates that most of the dissociative population on two different states end at the same kinetic energy.

As mentioned in the introduction, the asymmetric electron localization requires the coherent superposition of the nuclear wave packets with same final kinetic energy but opposite parities. Therefore, the close KER distributions shown in Fig. 2 will lead to the significant enhancement of the electron localization. To demonstrate this, in the following we investigate the electron localization in the dissociation of H_2^+ by the single

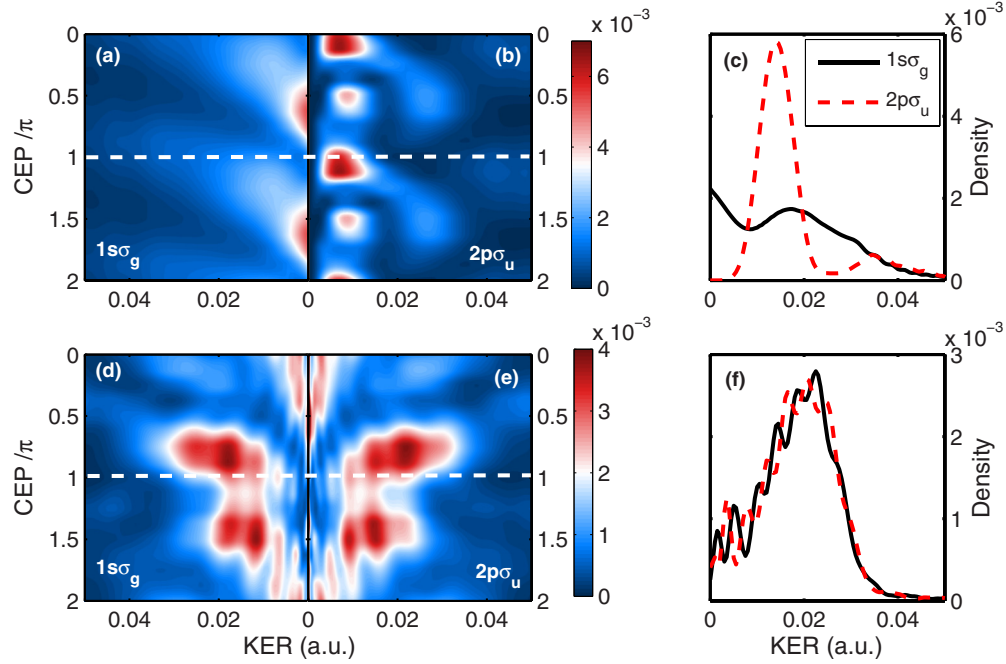


FIG. 2. (Color online) (a) and (b) show the KER distributions of the $1s_g$ and $2p_u$ states as a function of CEP in the single mid-infrared field, respectively. (c) Cut for the CEP of $\phi = 0\pi$, indicated by the dashed line in (a) and (b). (d)–(f) are the same as (a)–(c), respectively, but for the synthesized field. The other laser parameters are the same as those in Fig. 1.

mid-infrared and the synthesized fields, respectively. To quantify the degree of the electron localization on two nuclei, the asymmetry parameter A is defined and obtained as follows. First, we calculate the time-dependent dissociative wave function during the evolution of the wave function by $\Psi_{DWP}(R, z; t) = \Psi(R, z; t) - \sum_{n=0}^{N-1} \langle v_n(R, z) | \Psi(R, z; t) \rangle v_n(R, z)$, with v_n as the vibrational bound states and $N = 21$ as the number of v_n in our model. Then, the time-dependent probabilities of the dissociative wave packets localized on the upper [$P_+(t)$] or lower [$P_-(t)$] nucleus can be estimated by integrating the corresponding regions of the grid as follows:

$$P_{+,-}(t) = \int_0^{10} dR \int_0^{\pm 10} dz |\Psi_{DWP}(R, z; t)|^2 + \int_{10}^{R_{\max}} dR \int_{\pm R/2-5}^{\pm R/2+5} dz |\Psi_{DWP}(R, z; t)|^2, \quad (3)$$

where R_{\max} corresponds to the boundary of R . The evolution of the wave function in the external field has been continued until $P_{+,-}(t)$ are converged after the pulse is off. Finally, the asymmetry of the final electron localization probability is obtained by

$$A = \frac{P_+(t_{\text{end}}) - P_-(t_{\text{end}})}{P_+(t_{\text{end}}) + P_-(t_{\text{end}})}, \quad (4)$$

with t_{end} as the time when the probabilities $P_{+,-}(t)$ become stable in our simulations.

Figures 3(a) and 3(b) show the final electron localization asymmetry A as a function of the CEP for the interactions of H_2^+ with the single mid-infrared and the synthesized pulses, respectively. By comparing the results in Figs. 3(a) and 3(b), a much more pronounced CEP-dependent asymmetry

of the electron localization can be observed in the case of a synthesized pulse, as we expected. To gain insight into the interaction dynamics, we present the asymmetry of the electron localization as a function of the CEP and the KER in Figs. 3(c) and 3(d), where $A(E_k, \phi) = S_+(E_k, \phi) - S_-(E_k, \phi)$. Here the KER spectra $S_{+,-}(E_k)$ are calculated by Fourier analysis of the real-space wave function with the bound states projected out [20]. The results in Figs. 3(c) and 3(d) show distinct difference of the electron localization between the single mid-infrared [Fig. 3(c)] and the synthesized [Fig. 3(d)]

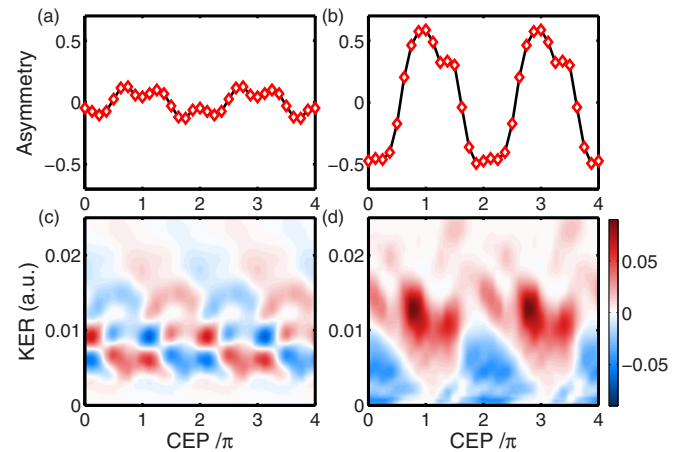


FIG. 3. (Color online) The CEP dependence of the final electron localization asymmetry in the (a) single mid-infrared pulse and (b) synthesized pulse. Also shown is the absolute asymmetry parameter $A(E_k, \phi)$ as a function of the CEP and the KER in the (c) single mid-infrared pulse and (d) synthesized pulse. The laser parameters are the same as those in Fig. 1.

pulses. In the single mid-infrared field, it is seen that maximal asymmetries around $E_k = 0.01$ and 0.02 a.u. are out of phase. This indicates that, at a given CEP, the electronic wave packets for different nuclear kinetic energies are localized on reverse directions, thereby smearing out the electron localization asymmetry, as shown in Fig. 3(a). In contrast, in the synthesized field [Fig. 3(d)], the KER distribution is modulated. The electron localization on the upper or lower nucleus is almost synchronous with the CEP, resulting in the enhancement of the localization asymmetry shown in Fig. 3(b).

Next, we discuss the role of the CEP in steering the electron during the dissociation. According to the KER spectra in Figs. 2(d) and 2(e), the dissociative population on two degenerate states end at the same kinetic energy for all phases and the yields of them are of almost the same amount. One might expect that in this case the electron should be only localized on the upper or lower nucleus, which means the asymmetry should change suddenly from 1 to -1 with the CEP. However, from Fig. 3(b) we can see that the localization asymmetry changes gradually with the CEP and, at some phases, the asymmetry is almost equal to zero. This is because the asymmetric electron localization also requires the spatial interference of the dissociative population. In order to make this interpretation more clearly, we calculate the R -dimensional probability distributions for the $1s\sigma_g$ and $2p\sigma_u$ states after the pulse is off. The CEP are chosen as $7/8\pi$ and $13/8\pi$, corresponding to the maximum and zero of the electron localization asymmetry in Fig. 3(b), respectively. The other laser parameters are the same as those in Fig. 1. Here are the calculation details. First, the wave function of the i th electronic state can be obtained by projecting the wave function to the electronic bound state $u_i(z; R)$ at each fixed internuclear distance, i.e.,

$$\Psi_i^P(z; R) = \langle \Psi_{DWP}(z; R) | u_i(z; R) \rangle u_i(z; R). \quad (5)$$

Here, i equals to 0, 1 and corresponds to the $1s\sigma_g$ and $2p\sigma_u$ states, respectively. The term $u_i(z; R)$ in Eq. (6) is the i th electronic bound wave function of H_2^+ at fixed internuclear distance, which can be obtained by solving the one-dimensional field-free Schrödinger equation in the imaginary time for H_2^+ in the Born-Oppenheimer approximation. Then, the R -dimensional probability of the i th electronic state can be estimated by

$$P_i(R) = \int_{-z_{\max}}^{z_{\max}} |\Psi_i^P(z, R)|^2 dz, \quad (6)$$

with z_{\max} as the boundary of z . Figure 4 shows the results for the CEP of $\phi = 7/8\pi$ [Fig. 4(a)] and $\phi = 13/8\pi$ [Fig. 4(b)], respectively. For $\phi = 7/8\pi$, we can see that most of the wave packets on the two states overlap in the region of $19 < R < 25$ a.u., leading to the pronounced asymmetry of the electron localization. However, for $\phi = 13/8\pi$, it can be seen that the peaks of the probability distributions for the $1s\sigma_g$ and $2p\sigma_u$ states are staggered and there is no significant overlapped region between them. As a result, the missed superposition in space of two states leads to the small asymmetry. Therefore, in our scheme, the spatial distributions of the population on two degenerate states are modulated by the CEP of the driven pulse, thereby resulting in the dependence of the electron localization on the CEP.

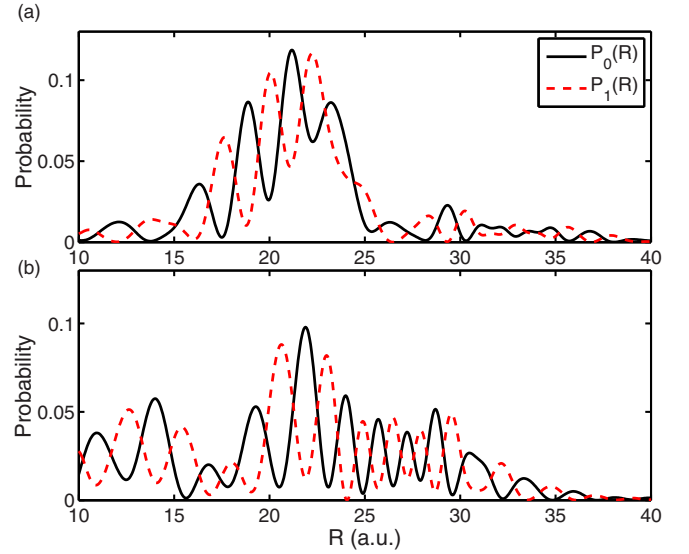


FIG. 4. (Color online) The R -dimensional probabilities for the $1s\sigma_g$ (the black solid curve) and $2p\sigma_u$ (the red [gray] dashed curve) states after the pulse is off. The CEP are $7/8\pi$ (a) and $13/8\pi$ (b), respectively. The other laser parameters are the same as those in Fig. 1.

Since the Stark shift of the lowest two states of H_2^+ is sensitive to the external static field, the manipulation of nuclear dynamics in our control scheme depends on the intensity of the low-frequency field. In Fig. 5(a) we show the localization asymmetry as a function of the intensity of the low-frequency

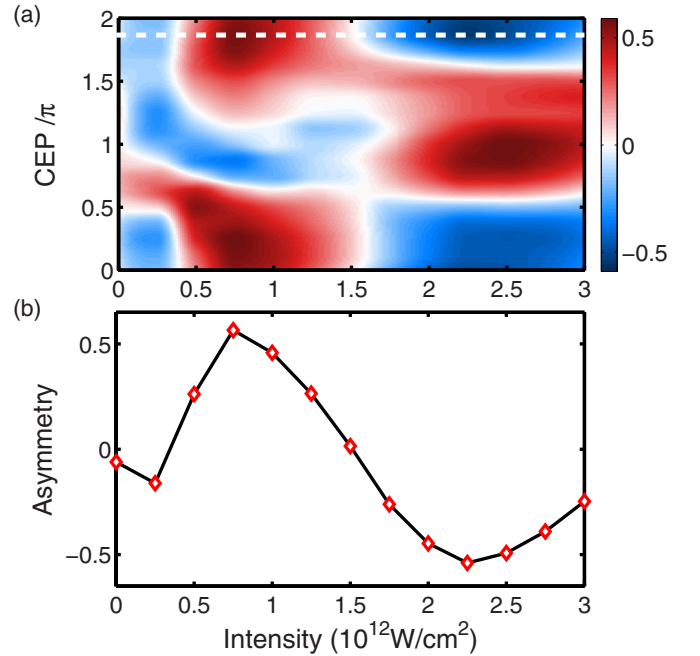


FIG. 5. (Color online) (a) The final asymmetry parameter of the electron localization as a function of the intensity of the low-frequency pulse and the CEP of the mid-infrared pulse. (b) Cut for the CEP of $\phi = 15/8\pi$, indicated by the dashed line in panel (a). The other laser parameters are the same as those in Fig. 1.

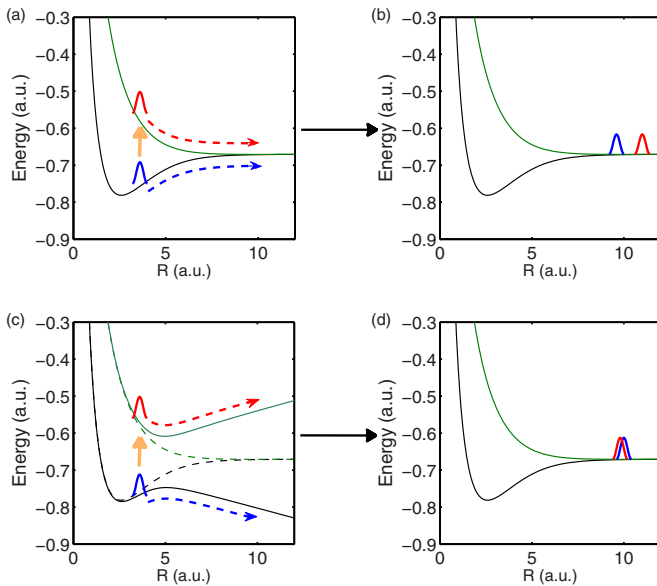


FIG. 6. (Color online) Schematic of the nuclear dynamics in the single mid-infrared field (top row) and in the synthesized field (bottom row). The arrows sketch the pathways of the nuclear wave packets during the dissociation.

pulse and the CEP of the mid-infrared pulse, while Fig. 5(b) is the cut at $\phi = 15/8\pi$. As we expected, the CEP-dependent electron localization changes with the intensity of the low-frequency pulse. For a fixed CEP, as shown in Fig. 5(b), the electron localization can be effectively controlled by tuning the intensity of the low-frequency pulse. This may offer a way to control the molecular fragments for the experiments even if the CEP is not exactly known. This will markedly relax the experimental requirements. However, if the intensity of the low-frequency pulse further increases, significant ionization will occur in the enhanced ionization region [8] and thereby weaken the electron localization. Therefore, in our scheme, the maximum of the intensity of the low-frequency pulse should be limited below $3 \times 10^{12} \text{ W/cm}^2$.

Finally, to gain an intuitive insight into the underlying dynamics in our scheme, we present in Fig. 6 a qualitative model of the dissociation mechanism responsible for the electron localization enhancement. In the dissociation of H_2^+ by a single mid-infrared field, the dissociative wave packets of two states propagate along the two molecular potential

surfaces, respectively. Because of the dipole selection rules, the dissociation pathways on these two states involve unequal net absorption numbers of photons. As a result, the wave packets of two states carry different final kinetic energies and can hardly interfere in space, as shown in Figs. 6(a) and 6(b). Thus, in this case the asymmetric electron localization is limited. However, by synthesizing a low-frequency field, the potential energy curves are dressed significantly due to the Stark effect. Then, the wave packets propagate along the dressed potential curves, as shown in Fig. 6(c). In this case, their kinetic energies will be modulated: For example, the wave packets on the ground state will be accelerated while those on the excited state will be decelerated. Therefore, most of the dissociative wave packets along two pathways will end at the same final kinetic energy and overlap in space, as shown in Fig. 6(d), leading to the enhancement of electron localization.

IV. CONCLUSION

In conclusion, we propose a method to efficiently steer the electron localization in dissociating H_2^+ by using the combination of a phase-stabilized few-cycle mid-infrared laser pulse and a low-frequency field. Different from the previous works, the mechanism behind the enhancement of the electron localization is that the dissociative population on two states is managed to end at the same kinetic energy and interference in space in our scheme. By adjusting the CEP, the dissociative population that shares the same kinetic energy can overlap in space, ultimately leading to the significant electron localization on one specific nucleus. We also show that the electron localization can be controlled by simply changing the intensity of the low-frequency field, which enables us to achieve the control even if the CEP is not exactly known, markedly relaxing the experimental requirements.

ACKNOWLEDGMENTS

This work was supported by the 973 Program of China under Grant No. 2011CB808103 and the National Natural Science Foundation of China under Grants No. 11404122 and No. 11234004. Numerical simulations presented in this paper were partially carried out using the High Performance Computing Center experimental testbed in SCTS/CGCL (see <http://grid.hust.edu.cn/hppc>).

- [1] A. Assion, T. Baumert, M. Bergt, T. Brixner, B. Kiefer, V. Seyfried, M. Strehle, and G. Gerber, *Science* **282**, 919 (1998).
- [2] C. Daniel, J. Full, L. González, C. Lupulescu, J. Manz, A. Merli, Š. Vajda, and L. Wöste, *Science* **299**, 536 (2003).
- [3] V. Roudnev, B. D. Esry, and I. Ben-Itzhak, *Phys. Rev. Lett.* **93**, 163601 (2004).
- [4] M. F. Kling, C. Siedschlag, A. J. Verhoef, J. I. Khan, M. Schultze, T. Uphues, Y. Ni, M. Uiberacker, M. Drescher, F. Krausz, and M. J. Vrakking, *Science* **312**, 246 (2006).
- [5] Y. Zhou, C. Huang, Q. Liao, and P. Lu, *Phys. Rev. Lett.* **109**, 053004 (2012); Q. Liao, Y. Zhou, C. Huang, and P. Lu, *New J. Phys.* **14**, 013001 (2012).
- [6] A. Baltuška, T. Udem, M. Uiberacker, M. Hentschel, E. Goulielmakis, C. Gohle, R. Holzwarth, V. Yakovlev, A. Scrinzi, and T. Hänsch, *Nature (London)* **421**, 611 (2003).
- [7] N. G. Kling, K. J. Betsch, M. Zohrabi, S. Zeng, F. Anis, U. Ablikim, B. Jochim, Z. Wang, M. Kübel, M. F. Kling, K. D. Carnes, B. D. Esry, and I. Ben-Itzhak, *Phys. Rev. Lett.* **111**, 163004 (2013).

- [8] K. Liu, P. Lan, C. Huang, Q. Zhang, and P. Lu, *Phys. Rev. A* **89**, 053423 (2014); C. Huang, P. Lan, Y. Zhou, Q. Zhang, K. Liu, and P. Lu, *ibid.* **90**, 043420 (2014).
- [9] K. P. Singh, F. He, P. Ranitovic, W. Cao, S. De, D. Ray, S. Chen, U. Thumm, A. Becker, M. M. Murnane, H. C. Kapteyn, I. V. Litvinyuk, and C. L. Cocke, *Phys. Rev. Lett.* **104**, 023001 (2010).
- [10] P. Lan, E. J. Takahashi, K. Liu, Y. Fu, and K. Midorikawa, *New J. Phys.* **15**, 063023 (2013).
- [11] F. He, *Phys. Rev. A* **86**, 063415 (2012).
- [12] Z. Wang, K. Liu, P. Lan, and P. Lu, *J. Phys. B* **48**, 015601 (2015).
- [13] V. Roudnev and B. D. Esry, *Phys. Rev. Lett.* **99**, 220406 (2007).
- [14] M. Kremer, B. Fischer, B. Feuerstein, V. L. B. de Jesus, V. Sharma, C. Hofrichter, A. Rudenko, U. Thumm, C. D. Schröter, R. Moshhammer, and J. Ullrich, *Phys. Rev. Lett.* **103**, 213003 (2009).
- [15] K. Liu, W. Hong, Q. Zhang, and P. Lu, *Opt. Express* **19**, 26359 (2011).
- [16] K. Liu, Q. Zhang, P. Lan, and P. Lu, *Opt. Express* **21**, 5107 (2013).
- [17] I. Znakovskaya, P. von den Hoff, G. Marcus, S. Zherebtsov, B. Bergues, X. Gu, Y. Deng, M. J. J. Vrakking, R. Kienberger, F. Krausz, R. de Vivie-Riedle, and M. F. Kling, *Phys. Rev. Lett.* **108**, 063002 (2012).
- [18] D. Ray, F. He, S. De, W. Cao, H. Mashiko, P. Ranitovic, K. P. Singh, I. Znakovskaya, U. Thumm, G. G. Paulus, M. F. Kling, I. V. Litvinyuk, and C. L. Cocke, *Phys. Rev. Lett.* **103**, 223201 (2009).
- [19] P. Lan, E. J. Takahashi, and K. Midorikawa, *Phys. Rev. A* **86**, 013418 (2012).
- [20] K. Liu, Q. Zhang, and P. Lu, *Phys. Rev. A* **86**, 033410 (2012).
- [21] F. He, C. Ruiz, and A. Becker, *Phys. Rev. Lett.* **99**, 083002 (2007).
- [22] Z. Jia, Z. Zeng, R. Li, Z. Xu, and Y. Deng, *Phys. Rev. A* **89**, 023419 (2014).
- [23] G. Sansone, F. Kelkensberg, J. F. Perez-Torres, F. Morales, M. F. Kling, W. Siu, O. Ghafur, P. Johnsson, M. Swoboda, E. Benedetti, F. Ferrari, F. Lepine, J. L. Sanz-Vicario, S. Zherebtsov, I. Znakovskaya, A. L'Huillier, M. Y. Ivanov, M. Nisoli, F. Martin, and M. J. Vrakking, *Nature (London)* **465**, 763 (2010).
- [24] E. P. Benis, M. Bakarezos, N. A. Papadogiannis, M. Tatarakis, S. Divanis, C. ÓBroin, and L. A. A. Nikolopoulos, *Phys. Rev. A* **86**, 043428 (2012).
- [25] F. Anis and B. D. Esry, *Phys. Rev. Lett.* **109**, 133001 (2012).
- [26] T. Y. Xu and F. He, *Phys. Rev. A* **90**, 053401 (2014).
- [27] B. Feuerstein and U. Thumm, *Phys. Rev. A* **67**, 043405 (2003).
- [28] K. C. Kulander, F. H. Mies, and K. J. Schafer, *Phys. Rev. A* **53**, 2562 (1996).
- [29] P. Lan, E. J. Takahashi, and K. Midorikawa, *Phys. Rev. A* **83**, 063839 (2011); J. Luo, Y. Li, Z. Wang, Q. Zhang, and P. Lu, *J. Phys. B* **46**, 145602 (2013); J. Luo, Y. Li, Z. Wang, L. He, Q. Zhang, P. Lan, and P. Lu, *Phys. Rev. A* **89**, 023405 (2014).
- [30] K. Liu, Q. Li, P. Lan, and P. Lu, *Mol. Phys.*, doi: 10.1080/00268976.2015.1015639.